ELSEVIER

Hearing Research 161 (2001) 35–44

HEARING RESEARCH

www.elsevier.com/locate/heares

Real time mapping of rat midbrain neural circuitry using auditory evoked potentials

M.F.D. Moraes [a], N. Garcia-Cairasco [b,*]

[a] *Physiology and Biophysics Department, Institute of Biological Sciences, Universidade Federal de Minas Gerais, Belo Horizonte, MG, Brazil*
[b] *Neurophysiology and Experimental Neuroethology Laboratory, Physiology Department, Ribeirão Preto School of Medicine, University of São Paulo, 14049-900 Ribeirão Preto, SP, Brazil*

Received 7 March 2001; accepted 26 June 2001

Abstract

Auditory evoked potentials were recorded in 360 homogeneously spaced sites, in a volume encapsulating the lateral lemniscus–inferior colliculus transition of anaesthetized rats, in order to calculate the electric field vector distribution with each moment in time referenced to the onset of sound presentation. Software, to conduct calculations and graphical representation, and hardware, to minimize neural damage upon recording, were developed in our laboratory. Our results indicate a smooth transition of both amplitude and direction of vectors, suggestive of sequentially activated sites with outward and inward ionic currents coherent with what is known of this part of the primary auditory pathway. That is, anatomical sites (neural generators) and latency for activation matches previous research of the auditory pathway, while adding a real time perspective to the anatomical substrates recruited during the auditory evoked response. An algorithm for calculating the divergent of the vector field, an estimate of the current source density inside the three-dimensional control volume, was used to infer the possible current sinks and sources generating the field potentials. This technique allowed a clear visualization of two distinct discharges arising from the lateral lemniscus towards the inferior colliculus, thus recording signal propagation, as a movie file, with 0.06 ms time resolution.

Key words: Electric field vector; Auditory evoked potential; Neural circuitry; Functional mapping

1. Introduction

Mapping brain activity in a time resolution compatible with the speed in which 'information' propagates throughout neural circuits is still an impossible task for non-invasive neuro-imaging techniques such as magnetic resonance imaging, computerized tomography, positron emission tomography and single photon computerized tomography. Activation itself is redefined accordingly to the technique used for recording (e.g. metabolical, electrical, neurochemical). This introduction focuses on the choice of electrophysiology as a high temporal resolution activity marker for neural circuits.

The electroencephalogram (EEG), discovered in the beginning of the century (Berger, 1929; Adrian and Matthews, 1934), records the electrical activity of neural populations throughout time and is still a widely used clinical examination tool for disorders involving the brain. The time-continued nature of EEG recordings permits the empirical association between the morphology of EEG data and behavior. However, if localization inferences are to be made as to which neural substrates are generating the field potentials recorded from scalp, even experts should carefully analyze EEG waveform, polarity and phase inversions in order to recognize true information and pitfalls (Jayakar et al., 1991).

* Corresponding author. Fax: +55 (16) 6330017.
E-mail address: ngcairas@fmrp.usp.br (N. Garcia-Cairasco).

Abbreviations: AEP, auditory evoked potentials; AP, antero-posterior; BERA, brainstem evoked response audiometry; CIC, central nucleus of the inferior colliculus; CSD, current source density analysis; ECIC, external nucleus of the inferior colliculus; EEG, electroencephalogram; EP, evoked potentials; EVF, electric vector field; IC, inferior colliculus; L, lateral; LL, lateral lemniscus; V, vertical

0378-5955/01/$ – see front matter
PII: S0378-5955(01)00341-0

As soon as breakthrough research in modelling biologically generated electrical signals at a cellular level emerged (Hodgkin and Huxley, 1952), better reasoning was possible regarding issues such as which portions of the brain were responsible for generating the electrical signals recorded from scalp electrodes (inverse problem of EEG). However, the generalization of cellular models of ionic current flow into more complex neural circuits was still subject to a great number of assumptions. One of the most prominent minds of the nineteenth century, H. Von Helmholtz, published an extensive study on electrical fields in volume conductors (Helmholtz, 1853) in which it is clear that the inverse problem of EEG is ill posed, in the sense that it has no unique solution. Therefore, even if we knew how to properly model the complex field potentials generated by neural networks working inside the brain, much reasoning would still be required to rule out the 'improbable' generators. The electric dipole theory is probably nowadays-best candidate for the reductionist modelling of neural network activity. Much work has been done in trying to develop algorithms to better localize intra-encephalic generators from scalp-recorded potentials in EEG (Magnus, 1961; Cuffin, 1995; Darcey et al., 1980; Kavanagh et al., 1978; Lesser et al., 1985; Wilson and Bayley, 1950; Wood, 1982). Although this could be a situation of practical limitations in clinical neurology, the 'gold standard' for EEG localization is still depth electrode placement (Spencer et al., 1982).

The use of field potential recordings inside encephalic structures during physiological activation of known neural circuitry is certainly a powerful tool on disclosing neural network functionality (Nicollelis et al., 1997), even though it has the inconvenience of being an invasive method. If field potential recordings are triggered by an external sensorial stimulus, then the EEG becomes an evoked potential (EP) recording. Considering the use of an auditory stimulus as trigger for the recording is named auditory evoked potentials (AEP). For a historical revision see Davis et al., 1939; Dawson, 1951, 1954; Liégeois-Chauvel et al., 1987.

The application of AEP in determining sites of 'activation' in a temporal sequence has been widely used for clinical purposes, e.g. brainstem evoked response audiometry (BERA). Mainly, BERA is useful for patients that cannot answer coherently to audiometric tests, for determining acoustic neurinomas and for the diagnostics of lesions in brain stem circuitry. However, the correlation of anatomical sites and specific waveforms distinguishable in the BERA pattern are still a matter under study (Biacabe et al., 2001), in spite of very elegant lesioning studies found throughout literature (Durrant et al., 1994; Funai and Funasaka, 1983). Most of these studies used conventional analysis, which involve the quantification of the whole AEP waveform pattern in terms of discrete parameters (e.g. latency and amplitude). The ideal set of parameters used for analysis of intra-encephalic AEP recordings should posses a similar continuous behavior in both space and time, as those observed for propagation itself, highlighting the dynamical characteristics of the signal (Moraes et al., 2000).

This work uses the EP technique while stimulating a known auditory neural circuit inside the mesencephalon of Wistar rats. AEP recordings are made inside a control volume that encapsulates the inferior colliculus (IC) and lateral lemniscus (LL). These recordings are used to calculate 360 electric field vectors, in the control volume, every 0.067 ms for as long as 20 ms after acoustic stimuli have been presented. The result is a neural circuit tracing technique, with high temporal resolution, capable of indicating the probable distribution of ionic currents inside a living brain processing information under physiological stimulation. Our choice of this specific portion of the auditory midbrain is an attempt to better disclose on the formation of wave III–V morphology of the BERA (Caird and Klinke, 1987). That is, to present a time-sequenced perspective on the complex interaction between brainstem circuitry that disallows a direct relationship between anatomical structures and BERA waveforms. A tone burst, instead of a click, was also chosen preferable in order to minimize the complexity of neural circuitry recruited.

The use of current source density (CSD) analysis, as an estimate for the divergent of the vector field, has proven to be effective for studying neural transmission in a one- or at most two-dimensional analysis of neural circuitry (Mitzdorf, 1985). The present report uses a mathematical algorithm for calculating a three-dimensional CSD analysis, although with a lower spatial resolution when compared to previous reports (Kandel and Buzsáki, 1997).

2. Materials and methods

2.1. Animals

The present study was conducted on eight adult Wistar rats from the main breeding stock of the Ribeirão Preto School of Medicine all weighting between 270 and 310 g. Rats were housed five per cage and submitted to an artificial lighting system, lights on at 07.00 h, lights off at 19.00 h, room temperature at 22°C, with free access to food (chow pellets; Nuvital, Brazil) and water. All procedures and experimental protocols were conducted in accordance with the Brazilian Society for Neuroscience and Behavior instructions for the use of animals in research.

2.2. Recording procedure

Data were collected by means of an array of three glass pipet-carbon fiber electrodes (Moraes and Garcia-Cairasco, 1997), 10 μm tip diameter, arranged in such a way as to be aligned and 1 mm apart. The reference electrode, stainless steel needle, was placed on the dorsal portion of the nasal bone. The monopolar/referential recording was then pre-amplified by a source follower circuit (field effect transistor SST201, SOT23) and amplified by a CyberAmp 320 Programmable Signal Conditioner (×10 000 gain, 30 Hz–5 kHz filter, notch filter 60 Hz; Axon Instruments, Inc). An analog/digital converter device at a sampling rate of 15 kHz (Biopac, Inc.; Acknowledge III) then converted the first 20 ms of the AEP response. For each recorded site, the computer saved the correspondent waveform of an average of 50 AEP recordings. After surgery, the rat, along with the electrode array and the stereotaxic, was placed inside a Faraday cage in order to minimize influence of external noise during recording.

The mapping procedure consisted of recording AEP on 360 different points, in a matrix formation as follows: 6 antero-posterior (AP) ×12 vertical (V) ×5 lateral (L). Stereotaxic coordinates were calculated with reference to the λ suture, for AP and L values, and with reference to the dura matter, for V values (Paxinos and Watson, 1997). The AP and V values ranged from 0.5 to −2.0 mm and 2.5 to 8.0 mm, respectively, all in 0.5 mm steps. The L values ranged from 1.0 to 3.0 mm, right hemisphere, also in 0.5 mm steps. Due to the linear configuration of the electrode array, and also the number of electrodes ($n = 3$) per array, a total of 10 V sweeps, through all 12 V sites, were necessary to cover the whole mapped volume (3 electrodes ×12 V sites ×10 sweeps = 360 points). Obviously, for each V sweep, the electrode array was inserted in the brain in such a way to cover the above-mentioned AP and L coordinates mapping.

2.3. Surgical procedure

All animals were anaesthetized with Thionembutal (Abbott, Brazil; 50 mg/kg) and properly positioned in the stereotaxic frame. The whole surgery and recording procedure were performed as fast as possible (2 h average time) to avoid further anaesthetic injection. Hypothermia induced by anesthesia was avoided by heating the rats during the recordings with a thermal bag, thus, temperature was maintained at 38 ± 2°C.

An adequate opening of the rat's skull was made with a dental drill in order to allow the mapping procedure described above. The sagittal sinus was carefully moved away from the electrode array insertion area by means of tensioning a surgical suture line that embraced the sinus according to Moraes and Garcia-Cairasco (1997). The dura mater was also removed from the electrode array insertion area and a solution of agar and saline was placed over the exposed portion of the encephalon in order to minimize dehydration. Before the agar solution was placed, the zero V coordinates were taken by lowering the electrode array until a sudden drop of resistance was detected between the electrode and the brain.

2.4. Acoustic stimulation

6 kHz tone bursts of 40 ms duration (70 dB) at a 2 Hz frequency were applied contra-laterally to the recording site through a hollowed stereotaxic auricular bar. The acoustic stimulation was also used to trigger the recording device for AEP synchronization.

2.5. Histology

Histological reconstruction of the recording sites was done by lesioning eight previously recorded positions at specific V, AP and L coordinates, beginning with the last recorded V column, in an attempt to mark all edges of the most medium and L faces of the mapped cube. The chosen lesioning coordinates were all possible combinations of L = 1 mm and 3 mm; V = 5 mm and 8 mm; AP = −0.5 mm and 2.0 mm. Animals were then injected with an anaesthetic overdose, perfused with saline (0.9%) and formaldehyde (4%), after which they were decapitated and the brain collected. 25 μm sections were stained with cresyl violet in order to highlight the lesion marks and the anatomical structures using the Paxinos and Watson (1997) stereotaxic atlas.

2.6. Data analysis

At the end of recording, each animal had a set of 360 averaged AEP waveforms recorded at specific sites. Each of these AEP waveforms was composed of 300 data values, once a sampling frequency of 15 kHz was used to digitize the 20 ms analog AEP signal. Each of these 300 sampled data values is the exact voltage (V_{sample}) recorded at a given latency (T_{sample}) after sound stimulus was presented.

$T\text{sample} = (n^{\text{th}}\ \text{sample})/300*20$ ms.

The electrical vector field (EVF), as a function of time, is determined by calculating the gradient of V_{sample}, on the entire mapped cube, at a specific T_{sample}. Note that every recorded point has an electric field vector associated to it (that varies in amplitude and direction with time), and the composition of all 360 electric field vectors makes the EVF.

A computer program was developed in Borland C++ 5.01 for Windows® in order to conduct all calculations

and graphical presentation of data. To better understand the algorithm used to calculate the EVF distribution in the control volume, let us exemplify the calculation procedure for one generic point inside the control volume, be this point S. Therefore, the voltage at point S, at time T_{sample}, is V_S. Through analogy, V_D is the voltage of the recorded point immediately dorsal to S, while V_V, V_A, V_P, V_M and V_L correspond respectively to voltage at points immediately ventral, anterior, posterior, medial and lateral to the anatomical site indicated by point S (Fig. 1C). Once the potential function V is discreetly recorded in time and space, the gradient of V becomes:

$$\vec{S} = \frac{(V_S - V_L) + (V_M - V_S)}{2} \bullet \vec{u}_{LM} + \frac{(V_S - V_A) + (V_P - V_S)}{2} \bullet \vec{u}_{AP} + \frac{(V_S - V_D) + (V_V - V_S)}{2} \bullet \vec{u}_{DV} \quad (1)$$

Where S is the electric field vector in point S; u_{LM}, u_{AP}, u_{DV} are respectively the unit vectors in directions latero-medial, antero-posterior, dorso-ventral. Fig. 1A illustrates an example of an artificially generated source (5 μV) in the external nucleus of the inferior colliculus (ECIC), with an analogous sink just ventral to it, while other points in the cube remained at 0 V, designed to test software behavior. The dot at the end of the vector (Fig. 1A) indicates the positive direction of the electric field, while the start of the vector lies upon one of the recorded sites. The anatomical correspondence of each recorded site is done by three-dimensionally rotating stereotaxic brain diagrams, as bitmap files, from an atlas (Paxinos and Watson, 1997). The computer software, although not shown here, is able to rotate the actual bitmap files from the digitized histological images, seen under a microscope, containing the lesion marks.

An EVF distribution, with electric field vectors calculated for each recorded anatomical site ($n = 360$), at a given time (T_{sample}), will be called from here on a CUBE. For the sake of clarity, there is a CUBE for each moment in time. In order to obtain a clear image of EVF distribution, digital filters were created so to avoid showing vectors that did not exceed a certain arbitrary value of 250 μV/mm. This cut-off value was chosen as twice the maximum vector encountered within the first 1 ms of recording, before acoustic 'information' arrived at any recorded points. A gain feature was also incorporated to the software in order to associate a desired number of pixels with vector amplitude.

An easy way to interpret the physical implication of the vectors in the EVF is to remember that it indicates the direction and intensity at which voltage is dropping. Therefore, if a positive ion such as Na^+ is positioned at a given recorded anatomical site, this ion would have the tendency of moving towards the direction expressed by the vector. Furthermore, if in one hand at any point of the recorded CUBE there is a convergence of electric field vectors, this point is most likely a current sink. On the other hand, if there is a divergence of electric field vectors, the point is most likely a current source (see Fig. 1 for an example).

With an algorithm very much like the one explained for the EVFs, the divergent of the three-dimensional vector field was calculated in order to highlight probable current sinks and sources. Eq. 2 indicates how current *Im* is calculated for each specific point of the vector field.

$$Im = \frac{(P_{LM}^{L} - S_{LM}) + (P_{LM}^{medial} - S_{LM})}{2} + \frac{(P_{DV}^{dorsal} - S_{DV}) + (P_{DV}^{ventral} - S_{DV})}{2} + \frac{(P_{AP}^{anterior} - S_{AP}) + (P_{AP}^{posterior} - S_{AP})}{2} \quad (2)$$

The lower script indicates the component of the vec-

Table 1
Parameter analysis of all recorded animals ($n = 8$)

Time interval (ms)	Localization of maximum			Vector module (0.2 mV/mm)	Moment of maximum (ms)
	AP (0–5)	V (0–11)	L (0–4)		
0.0–0.5	2.0 ± 1.2	4.5 ± . 3.5	1.5 ± 2.1	0.5 ± 0.1	0.3 ± 0.1
3.0–3.5	1.9 ± 1.2	9.9 ± 1.2	3.8 ± 0.7	6.6 ± 2.7	3.34 ± 0.08
5.0–5.5	2.0 ± 1.3	7.3 ± 2.0	3.1 ± 1.5	3.4 ± 1.4	5.2 ± 0.2
5.5–6.0	2.3 ± 1.4	5.8 ± 1.5	2.6 ± 1.8	2.9 ± 1.1	5.8 ± 0.2
7.0–7.5	2.5 ± 1.8	4.1 ± 0.8	1.9 ± 1.9	2.4 ± 0.9	7.2 ± 0.2

The maximum vector (in module) was determined for each 0.5 ms time segment for every animal of the experimental group. Summarization of the results of the eight rats used in the experiment. AP, V and L are the spatial coordinates in which such maximum occurred. Observe that at 3–3.5 ms time interval, the signal was at the level of the LL, while at 5–6 ms the signal progressed to the IC.

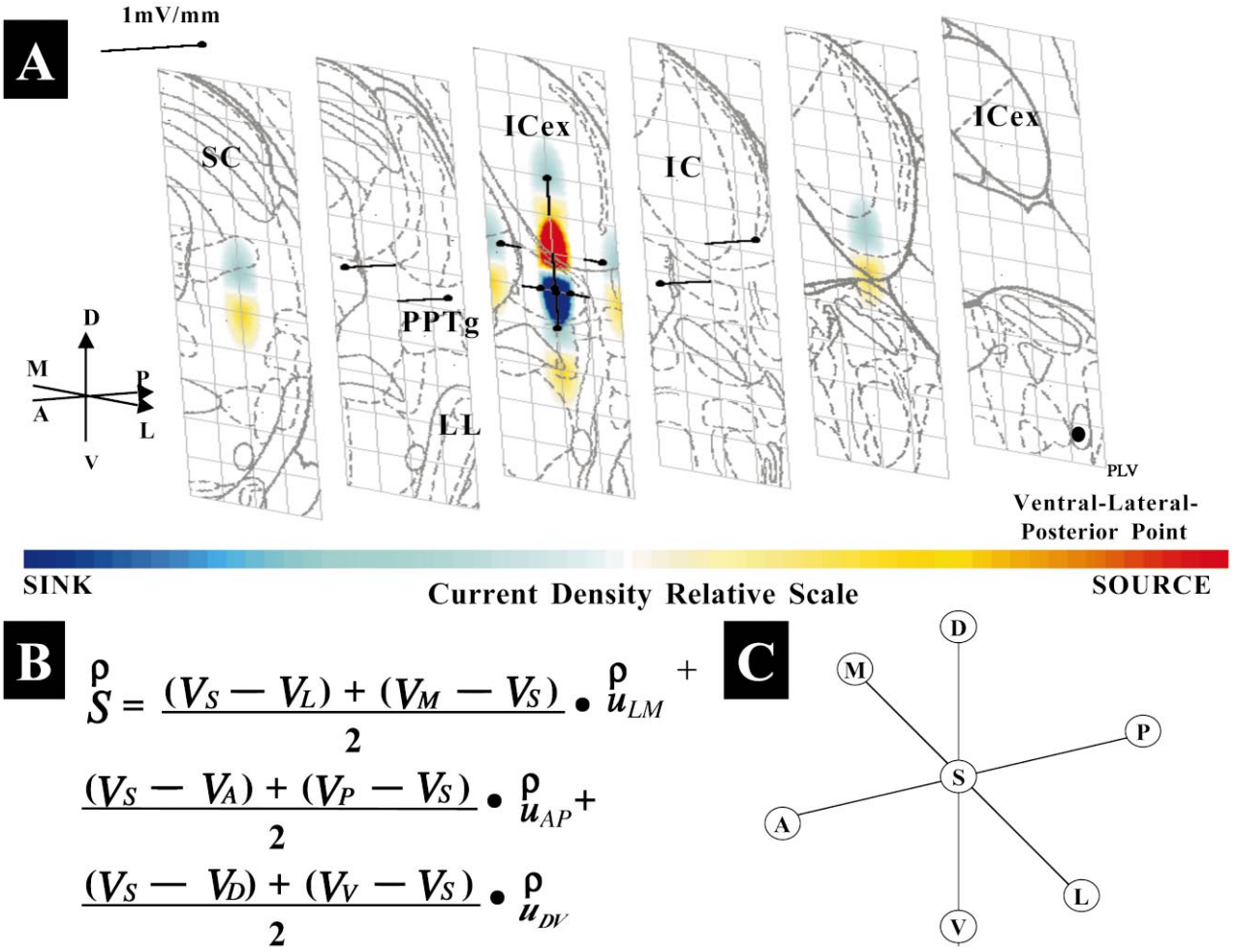

Fig. 1. Construction of the EVF distribution in a CUBE. (A) Artificially generated sink/source. An imaginary dipole was generated in the ECIC [5 mV (dorsal)/−5 mV (ventral)], while the rest of the points were maintained constant at 0 mV. The arrows, with dots at their end tips, indicate EVFs amplitude and direction. Notice the divergence of all arrows surrounding the point of positivity, region indicated by a red color indicative of a source. The arrows may as well be interpreted as a tendency for the direction of movement of positive-charged particles. (B) Mathematical formula used in the calculation of a generic vector located at point S. Indexes V, D, A, P, and M meaning respectively ventral, dorsal, anterior, posterior, and medial. (C) Shows the spatial distribution of the notation letters used in (B). A calibration vector of 1 mV/mm has been added to this and to all the following figures in order to quantify the EVFs.

tor in the anterior-posterior (AP), latero-medial (LM) and dorso-ventral (DV) axis coordinates. *S* is the vector for the reference point in which *Im* is being calculated, while *P* refers to vectors adjacent to this point. The upper script of *P* indicates the adjacent point used for calculation as lateral, medial, ventral, dorsal, anterior and posterior to the reference point.

Such inferences, regarding intra-encephalic currents and electric field vectors, have to be seen with restrictions due to media heterogeneities (Witwer et al., 1972). Nevertheless, the sinks and sources are color-coded represented over the EVFs distribution (see Mitzdorf, 1985 for more details in calculating relative sinks and source currents using CSD). An interpolation method was used to represent gradual color changes between recorded points of the vector field.

3. Results

Vectors of the EVF were calculated for every given time ($n = 300$, with a 0.0666 ms time resolution) at all recorded sites ($n = 360$ recorded anatomical sites) separately for each animal ($n = 8$); that is, 300 CUBEs per animal. All animals presented similar results, with same timing and position of activated nuclei, although the mapping procedure was for some animals displaced a millimeter off in any of the three spatial axes. Table 1 shows the averages and standard deviations of some parameters calculated within predefined time intervals.

If all 300 CUBEs from a specific animal were presented sequentially, in a form analogous to that of cartoon making, the observer has the dynamical idea of EVF pointing to moving sinks and sources along the

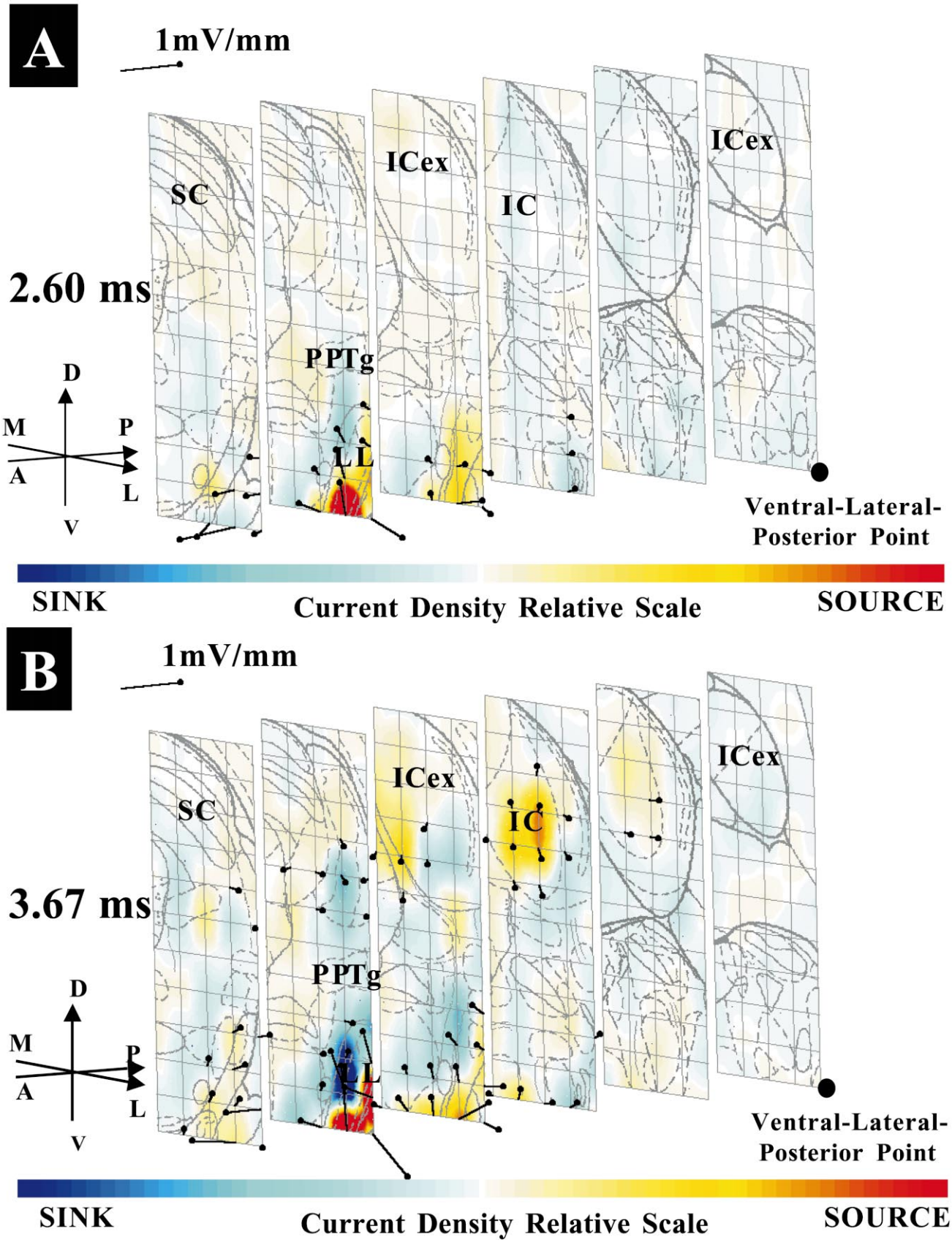
A
1mV/mm
SC
ICex
IC
ICex
2.60 ms
PPTg
LL
D
M
P
A
L
V
Ventral-Lateral-
Posterior Point
SINK
Current Density Relative Scale
SOURCE
B
1mV/mm
SC
ICex
IC
ICex
3.67 ms
PPTg
LL
D
M
P
A
L
V
Ventral-Lateral-
Posterior Point
SINK
Current Density Relative Scale
SOURCE

Fig. 2. Refer to Fig. 1 for legend details. The white to red colors highlight current sources, while the white to blue highlight current sinks. A calibration vector of 1 mV/mm has been added to the figures. Only vectors above the threshold filter of 250 μV/mm were plotted. (A) Recording of CUBE, animal R18, at time 2.6 ms after stimuli presentation. No vectors were observed before 2.5 ms. Observe a source in the LL prior to any other activity elsewhere in the recorded portion of the mesencephalon. (B) Recording of CUBE, animal R18, at time 3.7 ms after stimulus presentation. There is a sink in more dorsal portions of the LL, while a source seems to appear in the CIC. A less evident sink can be noted in the external IC nuclei towards the superior colliculus (SC).
←

primary auditory pathway. A computer animation of such sequentially presented frames is available in the form of electronic media, a movie file linked to this report (Web reference for the movie file www.icb.ufmg.br/~mfdm/hearingresearch). Due to the impossibility of showing in this report the whole time evolution of all 300 CUBEs per animal, we had to compromize by showing specific CUBEs that would approximately give the dynamic impression of sequential activation of the auditory pathway.

Figures 2A,B and 3A,B show CUBEs from rat 18 at times T = 2.6 ms, 3.73 ms, 4.93 ms and 5.73 ms, respectively. The white to red colors highlight current sources, while the white to blue highlight current sinks. Before 2.4 ms and after 10.0 ms, no electric field vector reached the cut-off criteria in the CUBE. As a whole, it can be easily noticed that signal processing travels pass through the LL, ECIC and central nucleus of the inferior colliculus (CIC).

4. Discussion

The CUBEs showed a sequential activation of neural substrates associated directly with auditory pathway (Ehret and Moffat, 1985; Huffman and Henson, 1990; Morest and Oliver, 1984; Servière et al., 1984) and at timings compatible with those found in literature (Funai and Funasaka, 1983; Caird et al., 1985; Caird and Klinke, 1987). One very important feature of the neural tracing system described here, the CUBE, is its high-resolution time detection of functional neural pathways in a three-dimensional space. Also, this work presents a much improved methodology, based upon physical properties of conducting volumes and bioelectrogenesis, when compared to previous work based upon empirical assumptions of wave-morphology and time-sequenced neural circuitry activation (Moraes et al., 2000). Thus, it is the authors' opinion that this paper improves significantly the coupling of neural substrates with specific waves from the clinically used BERA, e.g. the AEP recorded from scalp. For example, we could identify two distinct discharges from the LL towards the IC in the 3–6 ms time window. Also, it was possible to visualize a concomitant activation of both IC and LL creating a resultant dipole that would be seen from scalp as a single waveform. The technique is far from disclosing the complexity of the inter-neural connections of the acoustic midbrain, however, it certainly enlightens the macrostructure of the dipoles being generated in the LL and IC during acoustic stimulation.

Other techniques have attempted to trace functional neural circuitries in a high-resolution temporal perspective, most of which are based on recording bioelectric-generated signals. The pure analysis of wave morphology, especially regarding amplitude and latency, does not derive very useful physiological information about the neural circuitry, as does the determination of proper distribution of electric field gradients or the CSD analysis (Mitzdorf, 1985). That is, voltage traces may reflect, through volume conduction, the activity of distant current generators and, therefore, are not reliable in determining the anatomical substrates of neural activity. An application of the CSD analysis, in inferring functional neural circuitry, appears in a paper by Kandel and Buzsáki (1997). In this report, recordings from somatosensory cortical layers, activated either by electrical stimulation or endogenous oscillators, showed remarkable similarity in their sink/source distribution, in spite of noticeable differences in voltage- versus depth profiles and latency of multi-electrodes. Thus, the authors draw some interesting considerations on intracortical circuits. However, CSD analysis is usually uni-dimensional, or at most bi-dimensional, making it very hard to visualize the flow of information throughout a three-dimensional neural circuit, as does the CUBE. The calculations made to determine the divergent of the EVF in the CUBE and which presented it as a color gradient may be interpreted, with caution, as a three-dimensional CSD. The sinks and sources determined by the color gradient assume that spatial sampling (0.5 mm) is low enough to consider the conductivity tensor isotropic and constant throughout the control volume, homogeneous media, which has implications on data analysis (Imoniemi, 1993; Nunez, 1981; Jefferys, 1995). The divergent of the EVF will be, in such case, proportional to the magnitude of current sinks or sources (Mitzdorf, 1985; Lopes da Silva and Rotterdam, 1993).

Single unit recording histograms also consider neural circuitry activation in a temporal perspective by assigning the recruitment of a specific nucleus to neural firing latency, although it still represents a single neuronal discharge. An uncountable number of reports have used this technique to highlight temporal dependency and, therefore, circuit connectivity between nuclei.

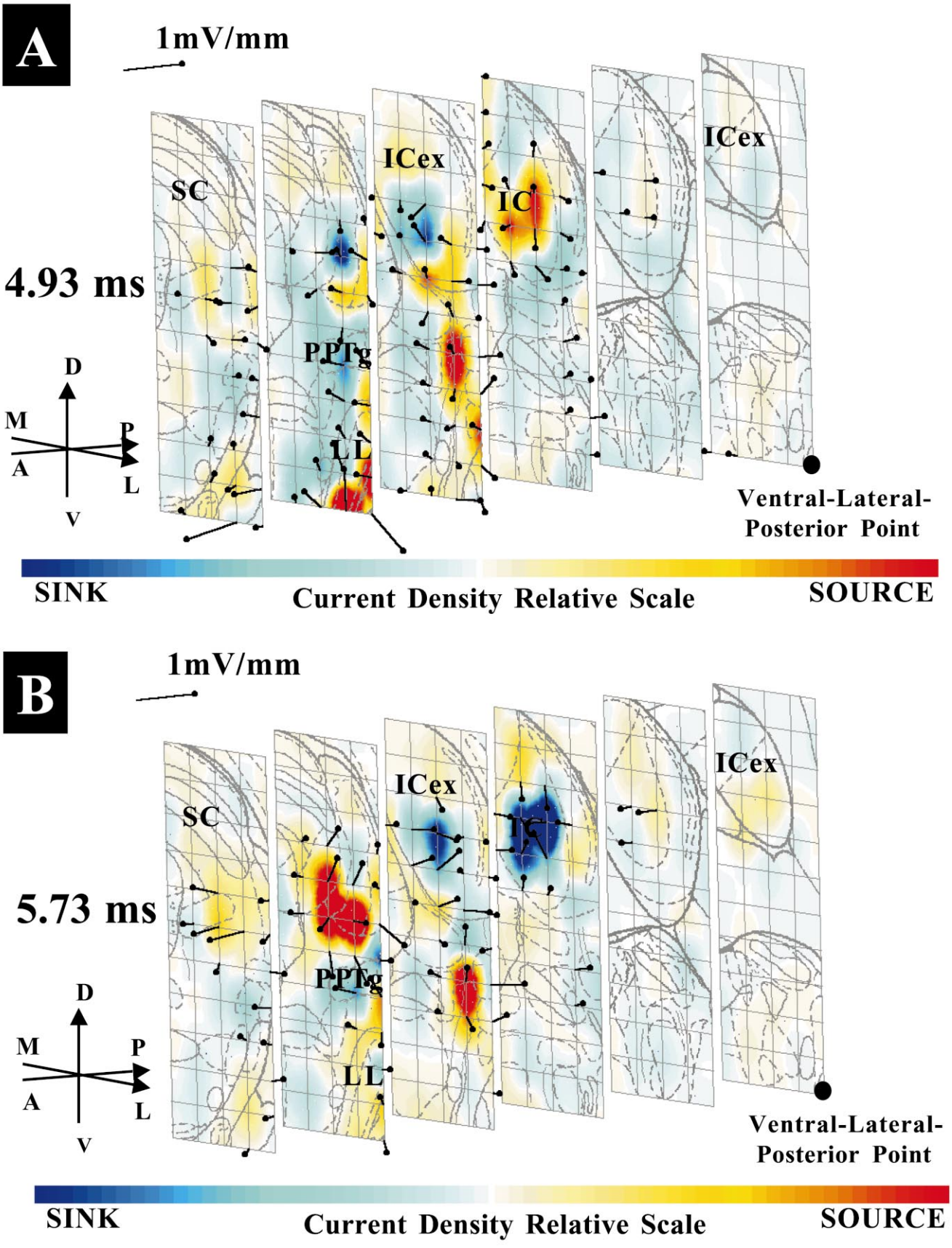
A
1mV/mm
SC
ICex
IC
ICex
4.93 ms
PPTg
LL
D
M
P
A
L
V
Ventral-Lateral-
Posterior Point
SINK
Current Density Relative Scale
SOURCE
B
1mV/mm
SC
ICex
IC
ICex
5.73 ms
PPTg
LL
D
M
P
A
L
V
Ventral-Lateral-
Posterior Point
SINK
Current Density Relative Scale
SOURCE

Fig. 3. Refer to Fig. 2 for legend details. (A) Recording of CUBE, animal R18, at time 4.9 ms after stimuli presentation. An evident sink is observed in the ECIC and deep mesencephalic tegmental area, while a source is located in the CIC. Notice the evolution of sinks throughout Figs. 2B and 3A,B and (B) Recording of CUBE, animal R18, at time 5.7 ms after stimulus presentation. There is a shift of sink from the IC external (A) to IC central nucleus (B) in less than 1 ms. The deep mesencephalic tegmental area is also a more prominent sink than in (B). The 'cartoon'-like evolution of sinks/sources is quite obvious if one observes Fig. 2B, (A) and (B) in sequence (see Web reference for the movie file www.icb.ufmg.br/~mfdm/hearingresearch).
←

One very elegant application, and technological development, of the single unit recording concept deserves special attention (Nicollelis et al., 1997). In this work, special digital signal processor chips are programmed to recognize and differentiate single firing waveform morphology of neurons located nearby an electrode tip, usually around four different neurons are recorded from a single electrode. The work suggests the existence of spatial/temporal discharge patterns from the recorded neurons, in different nuclei, to be correlated with physiological function. This technique is an indirect analysis of neural circuitry processing, different from the CUBE, but nevertheless a brilliant approach for understanding neural circuitry ultimate function.

Recorded field potential evoked responses, coupled with lesion of suggestive neuroanatomical circuits (derived from anatomical neural-tracer techniques), have also shown to be very effective in analyzing neural circuits in a high temporal perspective (Legatt et al., 1986; Funai and Funasaka, 1983). The inconvenience of using parameters such as voltage intensity and waveform latency, recorded inside a volume conductor, is as applicable here as it was while discussing the CSD technique (second paragraph of this section). Furthermore, visualization of information flow throughout a specific three-dimensional neural circuit, from parameters such as potential amplitude or waveform latency, is a matter of great abstraction and training. In fact, some peaks, which are interpreted as activity from nuclei and as source for that peak activity, could have their origin in bends of the activated fiber tracts, leading to misinterpretation of evoked response waveform. The technique presented here could be applied to visualize activated nuclei as well as the fiber tract pathway in a high temporal/spatial perspective in experimental models capable of providing inverse problem EEG algorithms (dipole source localization algorithms) with important feedback.

Some of the current sink/source distribution found in Figs. 2B and 3 resemble the hypothetical single neuron case presented in electrophysiology textbooks (Niedermayer and Lopes da Silva, 1993; see Lopes da Silva and Rotterdam, 1993). The example of excitatory apical dendritic synaptic activity inducing a sink at the synaptic cleft, while a passive source is generated towards the cell soma is analogous to the net result observed in Figs. 2B or 3 from the LL-ECIC and CIC. This hypothetical scenario is strengthened once the CIC becomes a sink a few milliseconds after it was a source (Fig. 3B), and no more signals are observed in more caudal portions of the auditory pathway.

The temporal perspective of signal evolution as well as the direct measurements of electric field vectors inside a reasonably large portion of the auditory mesencephalic area are important factors on understanding the net result of neural circuitry activation. Ongoing experiments are using endogenous spike activity from epileptic animal models to trigger recording, analogous to the EP technique, of CUBEs in suggested areas that may contain epileptogenic neural circuits.

Independently of the recording matrix array used here, important information about source localization may be derived by using a not so elaborate electrode array implanted inside the brain. For example, a simple triangulation methodology can be used to infer 'dipole' source localization from at least three different electric field vectors in a non-linear arrangement. These direct measurements of samples of the EVF, with further studying and technological improvement, could feedback the inverse problem algorithms in such a way that, for some specific situations, regarding specific neural disorders, the electrical dipole theory may not be the paradigm of choice for source localization. And even in those cases in which the dipole theory applies nicely, direct measurements of EVF in experimental conditions may contribute to the development of better mathematical algorithms or models for human EEG source localization of dipoles. Nevertheless, invasive electrophysiology would hardly apply for normative clinical examinations. However, once this technique shows its validity in experimental animals, it could be candidate for certain extreme cases, e.g. epilepsy neurosurgery, in which the visualization of the evolution of activated nuclei and fiber pathway is of relevance. There are currently available, for experimental animals, electrode arrays with several points of recording along a very thin strip (Kandel and Buzsáki, 1997). This setup would allow a much faster recording of an EVF distribution and less neural damage.

Acknowledgements

To Brazilian Foundations FAPESP (Grants 92/4464-3, 93/2023-2 and 99/06756-0) and CNPq (Grants 521596/94 and 521697/96-4) for financial support.

N.G.-C. and M.F.D.M were recipients of CNPq and CAPES-Brazil fellowships.

References

Adrian, E.D., Matthews, B.H.C., 1934. The Berger rhythm: potential changes from the occipital lobes in man. Brain 5, 355–385.

Berger, H., 1929. Uber das Elektrenkephalogramm des Menschen. 1st report. Arch. Psychiatr. Nervenkrankh. 87, 527–570.

Biacabe, B., Chevallier, J.M., Avan, P., Bonfils, P., 2001. Functional anatomy of auditory brainstem nuclei: application to the anatomical basis of brainstem auditory evoked potentials. Auris Nasus Larynx 28, 85–94.

Caird, D.M., Klinke, R., 1987. The effect of inferior colliculus lesions on auditory evoked potentials. Electroencephalogr. Clin. Neurophysiol. 68, 237–240.

Caird, D., Sontheimer, D., Klinke, R., 1985. Intra- and extracranially recorded auditory evoked potentials in the cat. I. Source location and binaural interaction. Electroencephalogr. Clin. Neurophysiol. 65, 50–60.

Cuffin, B.N., 1995. A method for localizing EEG sources in realistic head models. IEEE Trans. Biomed. Eng. 42, 68–71.

Darcey, T.M., Ary, J.P., Fender, D.H., 1980. Methods for the localization of electrical sources in the human brain. Prog. Brain Res. 54, 128–134.

Davis, H., Davis, P.A., Loomis, A.L., Harvey, E.N., Hobart, G., 1939. Electrical reactions of the human brain to auditory stimulation during sleep. J. Neurophysiol. 2, 500–514.

Dawson, G.D., 1951. A summation technique for detecting small signals in a large irregular background. J. Physiol. 115, 2P–3P.

Dawson, G.D., 1954. A summation technique for the detection of small evoked potentials. Electroencephalogr. Clin. Neurophysiol. 6, 65–84.

Durrant, J.D., Martin, W.H., Hirsh, B., 1994. 3CLT ABR analyses in human subject with unilateral extirpation of the inferior colliculus. Hear. Res. 72, 99–107.

Ehret, G., Moffat, A.J.M., 1985. Inferior colliculus of the house mouse. J. Comp. Physiol. 156, 619–635.

Funai, H., Funasaka, S., 1983. Experimental study on the effect of inferior colliculus lesions upon auditory brain stem response. Audiology 22, 9–19.

Helmholtz, H., 1853. Über einige gesetze der vertheilung elektrischer ströme in körperlichen leitern, mit anwendung auf die thierisch-elekstrischen versuche. Ann. Phys. Union Chem. 29, 211–377.

Hodgkin, A.L., Huxley, A.F., 1952. A quantitative description of membrane current and its application to conduction and excitation in the nerve. J. Physiol. 117, 500–544.

Huffman, R.F., Henson, O.W., Jr., 1990. The descending auditory pathway and acousticomotor systems: connections with the inferior colliculus. Brain Res. Rev. 15, 295–323.

Imoniemi, R.J., 1993. Models of source currents in the brain. Brain Topogr. 5, 331–336.

Jayakar, P., Duchowny, M.S., Resnick, T.J., Alvarez, L.A., 1991. Localization of seizure foci: Pitfalls and caveats. J. Clin. Neurophysiol. 8, 414–431.

Jefferys, J.G., 1995. Nonsynaptic modulation of neuronal activity in the brain: electric currents and extracellular ions. Physiol. Rev. 75, 689–723.

Kandel, A., Buzsáki, G., 1997. Cellular-synaptic generation of sleep spindles, spike-and-wave discharges, and evoked thalamocortical responses in the neocortex of the rat. J. Neurosci. 17, 6783–6797.

Kavanagh, R.N., Darcey, T.M., Lehmann, D., Fender, D.H., 1978. Evaluation of methods for three-dimensional localization of electrical sources in the human brain. Trans. Biomed. Eng. 25, 421–429.

Legatt, A.D., Arezzo, J.C., Vaughan, H.G., Jr., 1986. Short-latency auditory evoked potentials in the monkey. II. Intracranial generators. Electroencephalogr. Clin. Neurophysiol. 64, 53–73.

Lesser, R.P., Lüders, H., Dinner, D.S., Morris, H., 1985. An introduction to the basic concepts of polarity and localization. J. Clin. Neurophysiol. 2, 45–62.

Liégeois-Chauvel, C., Chauvel, P., Marquis, P., Musolino, A., Bancaud, J., 1987. Intra-cerebral recordings of primary auditory evoked potentials in man. In: Engel, J. (Ed.), Fundamental Mechanisms of Human Brain Function. Raven Press, New York, pp. 39–49.

Lopes da Silva, F.L., Rotterdam, A.V., 1993. Biophysical Aspects of EEG and Magnetoencephalogram Generation. Electroencephalography Basic Principles, Clinical Applications, and Related Fields, 3rd edn. Williams and Wilkins, Baltimore, MD, 78–91.

Magnus, O., 1961. On the technique of localization by electroencephalography. Electroencephalogr. Clin. Neurophysiol. 13 (Suppl.), 1–35.

Mitzdorf, U., 1985. Current source-density method and application in cat cerebral cortex: investigation of evoked potentials and EEG phenomena. Physiol. Rev. 65, 37–100.

Moraes, M.F.D., Del Vecchio, F., Terra, V.C., Garcia-Cairasco, N., 2000. Time evolution of acoustic information processing in the mesencephalon of Wistar rats. Neurosci. Lett. 284, 13–16.

Moraes, M.F.D., Garcia-Cairasco, N., 1997. Glass-pipette-carbon fiber micro electrodes for evoked potential recordings. Braz. J. Med. Biol. Res. 30, 1319–1324.

Morest, D.K., Oliver, D.L., 1984. The neuronal architecture of the inferior colliculus in the cat: defining the functional anatomy of the auditory midbrain. J. Comp. Neurol. 222, 209–236.

Nicollelis, M.A., Ghazanfar, A.A., Faggin, B.M., Votaw, S., Oliveira, L.M., 1997. Reconstructing the engram: simultaneous, multisite, many single neuron recordings. Neuron 18, 529–537.

Niedermayer, E., Lopes da Silva, F., 1993. Electroencephalography: Basic principles, clinical applications, and related fields, 3rd edn. Williams and Wilkins, Baltimore, MD.

Nunez, P.L., 1981. Electrical Fields of the Brain. Oxford Press, New York.

Paxinos, G., Watson, C.H., 1997. The Rat Brain in Stereotaxic Coordinates. Academic Press, Sidney.

Servière, J., Webster, W.R., Calford, M.B., 1984. Iso frequency labelling revealed by a combined 2-[^{14}C]-deoxyglucose, electrophysiological and horseradish peroxidase study of the inferior colliculus of cat. J. Comp. Neurol. 288, 463–477.

Spencer, S.S., Spencer, D.D., Williamson, P.D., Mattson, R.H., 1982. The localizing value of depth electroencephalography in 32 patients with refractory epilepsy. Ann. Neurol. 12, 248–256.

Wilson, F.N., Bayley, R.H., 1950. The eletric field on an eccentric dipole in a homogeneous spherical conducting medium. Circulation 1, 84–92.

Witwer, J.G., Trezek, G.J., Jewett, D.L., 1972. The effect of media inhomogeneities upon intracranial electrical fields. IEEE Trans. Biomed. Eng. 19, 352–362.

Wood, Ch.C., 1982. Application of dipole localization methods to source identification of human evoked potentials. Ann. N.Y. Acad. Sci. 388, 139–155.